PHYSICAL REVIEW C VOLUME 15, NUMBER 3 MARCH 1977

Electroproduction and photoproduction of charged pions on ^{27}Al and ^{51}V at intermediate energies

I. Blomqvist, P. Janeček, and G. G. Jonsson
Department of Nuclear Physics, Lund Institute of Technology, Sölvegatan 14, S-223 62 Lund, Sweden

H. Dinter and K. Tesch
Deutsches Elektronen-Synchrotron, DESY, Hamburg, West Germany

N. Freed and P. Ostrander
Department of Physics, Pennsylvania State University, University Park, Pennsylvania 16802
(Received 30 August 1976)

Cross sections for electroproduction and photoproduction of charged pions on ^{27}Al and ^{51}V have been measured in the energy region 130–580 MeV by use of the activation method. Special care has been taken to subtract out background yields. Photoproduction cross sections have been calculated from the region just above threshold to the tail of the (3,3) resonance. π-nucleus final state interactions are taken into account through optical potentials. Calculated photoproduction cross sections are decomposed into multipoles which are used to derive relative bremsstrahlung-induced to electron-induced yields. The pronounced effect of final state interactions is pointed out and discussed.

[NUCLEAR REACTIONS ^{27}Al(γ,π^+), ^{27}Al$(e,e'\pi^+)$, ^{51}V(γ,π^+), ^{51}V$(e,e'\pi^+)$, ^{51}V(γ,π^-), ^{51}V$(e,e'\pi^-)$. Activation method. E_0=130–580 MeV; measured σ_q and σ_e, deduced σ_k; calculated σ_k and σ_q/σ_e. Ge(Li) detector.]

I. INTRODUCTION

The processes of pion electroproduction and photoproduction on nuclei are of interest from two points of view. First, they can shed light on various structural features of the nuclei involved and, second, they can provide information on the π-nucleus interaction supplementary to that obtained from pion scattering experiments. Within the energy range of the outgoing pion, two regions have come in for careful study. In the region just above threshold the reaction is dominated by s-wave production.[1] In addition, details of the weak π-nucleus final state interactions (fsi) are obtainable from low-energy scattering and mesonic atom data.[2] In spite of these simplifications, the situation at threshold is far from clear since significant discrepancies often occur between theory and experiment.[1,3] These discrepancies have been attributed to incorrect application of soft-pion theorems[4] in deriving the single-nucleon production amplitude,[5] to errors in the determination of nuclear form factors from electron scattering,[6] to experimental inaccuracies,[7] and to other sources.[8]

The second region of interest is that of the (3,3) resonance. In contrast to threshold production, in which the residual nucleus is almost transparent to pions, there exists in this region a strong p-wave reabsorption which considerably attenuates the pion wave function. Furthermore, the analysis is complicated by the need to include momentum-dependent terms in the single-nucleon production amplitude and an often considerable number of pion partial waves. These difficulties are more than offset, however, by the possibility of elucidating details of the π-nucleus interaction in the energy region in which it is strongest and changes most rapidly.

In this paper we will calculate pion photoproduction cross sections from the region just above threshold to the tail of the (3,3) resonance, taking into account fsi between the pion and daughter nucleus. All momentum-dependent terms in the production amplitude and all contributing pion partial waves will be retained. The calculated photoproduction cross sections will then be decomposed into contributing multipoles from which relative yields of bremsstrahlung-induced to electron-induced reactions will be calculated using the method of Dalitz, Yennie, and Barber.[9] Our results for the reactions ^{27}Al$(\gamma,\pi^+)^{27}$Mg, ^{51}V$(\gamma,\pi^+)^{51}$Ti, and ^{51}V$(\gamma,\pi^-)^{51}$Cr and the corresponding σ_q/σ_e ratios will be compared to the results of activation measurements which we have carried out at the electron linac at Deutsches Elektronen Synchrotron (DESY). In such measurements only those reaction channels are open which lead to bound states of the residual nucleus. It is worth pointing out that although a number of photoproduction experi-

ments were carried out earlier in these mass and energy regions,[10-17] the results were seldom consistent with each other. The most likely source of disagreement lies in the neglect or underestimation by earlier authors of background reactions within the target. In the present work we found that these background yields were of the same magnitude as the pion-production yields. It was possible, however, to separate out the background contributions by measuring the yields of separate foils in stacks with varying total thicknesses. Our final results often differ substantially from other recent measurements.

Details of the experiments and a summary of the findings will be described in Secs. II and III. An outline of the theory and calculations is contained in Sec. IV. Comparison between theory and experiment is given in Sec. V. A final summary and conclusions are contained in Sec. VI.

II. EXPERIMENTAL DETAILS

A. Irradiations and measurements

The experiments were carried out at the electron linear accelerator LINAC II at DESY in Hamburg. The electron beam was directed into a side room of the accelerator building by an energy-defining transport system. The beam intensity was 5×10^{13} e/s with $\Delta E/E\sim1\%$. The vacuum pipe terminated 40 cm in front of the target. Before reaching the target, the beam had to penetrate the vacuum foil [5×10^{-3} cm of steel, corresponding to about 2.8×10^{-3} radiation lengths (r.l.)], a fluorescent screen (3.5×10^{-4} r.l.), and the air gap (1.4×10^{-3} r.l.). The beam intensity was measured by a secondary emission monitor placed behind the target. This monitor was in turn calibrated by a Faraday cup. The beam diameter was about 1 cm. By measuring the activity of aluminum foils exposed perpendicular to the electron beam, we determined the profile to distances at which the intensity had dropped to 10^{-3} times peak intensity. From this determination we concluded that the room background could be safely neglected.

The targets consisted of stacks of square foils (3×3 cm^2) of Al and V, having thicknesses of 1.7×10^{-3} r.l. and 4.7×10^{-3} r.l., respectively. The target materials were of high purity ($\geq99.9\%$).

The aluminum samples were irradiated at 20 electron energies in the energy range 131–577 MeV, the exposures lasting about 15 min. Vanadium was irradiated at 14 energies in the same energy range, both 10 min and 3 h exposures being carried out at each energy. After the irradiation, the γ activity in the foils was measured with a 60 cm^3 Ge(Li) detector. The first measurement began within 5 min of the end of the irradiation. Decay data were taken from Ref. 18.

The solid angle between foil and detector was measured by use of a radioactive sample of known activity.

B. Analysis of experimental data

When a stack of thin foils is irradiated with electrons of energy E_0, it can be shown[19] that the yield Y is a linear function of the target thickness

$$Y(E_0,\tau)=\sigma_e(E_0)+\sigma_q(E_0)C(E_0)\tau, \tag{2.1}$$

where σ_e is the electron cross section, σ_q the bremsstrahlung cross section per equivalent quantum, and τ is the target thickness in r.l. The correction factor $C(E_0)$ depends on the shape of the bremsstrahlung spectrum and certain corrections in the expression for the radiation length.[19] Its magnitude was found to be 0.8–0.9 in our energy region. From Eq. (2.1) it follows that σ_e and σ_q can be determined simultaneously by studying the yield versus target thickness.

This technique has been used in the past by many authors. However, for pion photoproduction and electroproduction measurements, Eq. (2.1) must be modified to take into account the background from (n,p) and (p,n) reactions induced by neutrons and protons produced in the target stack. By measuring the yields of successive foils in stacks with various total thicknesses (≤10 foils) at the same energy E_0, we are able to separate out the background contribution. For π^+ production reactions it is possible to calculate analytically the amount of (n,p) contamination in every foil. Calculations were carried out for circular foils having the same area as the square target foils. This substitution should constitute a good approximation and the geometry is easier to handle.

The following assumptions were made in the calculations (details of the calculations are given in Ref. 19):

(1) The electron intensity is constant over the irradiated area.

(2) Neutron yield in the stack varies with stack depth according to Eq. (2.1).

(3) The neutrons produced have an angular distribution proportional to $(1+\beta\cos\theta)$, where θ is the lab angle between the neutron direction and the incident electron beam.

(4) The mean free path of the neutrons is sufficiently long that the number of (n,p) reactions in a given foil is proportional to the total distance the neutrons have to pass through in that foil (i.e., multiple scattering effects are ignored).

The calculated background will therefore contain two free parameters. One is the scale factor gotten from the (γ,n), $(e,e'n)$, and (n,p) cross

sections in the nucleus under study; the other is the angular distribution parameter β. These parameters can be determined from a least-squares fit to the measurements below pion threshold where only the (n,p) reaction contributes to the yield. Figure 1 shows the yield of ^{27}Mg for successive foils in stacks of various total thickness at $E_0 = 131$ MeV. Open circles are experimental data and solid curves are calculated background yields fitted to the experimental points. It is seen that both relative yields and variation of yields with depth in the various stacks are well reproduced.

To extrapolate the (n,p) background to energies above pion threshold it is necessary to determine its energy dependence. Since the neutron production is dominated by the giant resonance and the (n,p) reaction peaks at low neutron energies,[20] it is reasonable to assume that only the scale factor changes when the electron energy is increased above pion threshold. We therefore made a least-squares fit of σ_e and σ_q and calculated a scale factor for the background at each electron energy. Since the scale factor was found to increase linearly with electron energy we fitted a straight line to the scale factor versus energy curve to eliminate small fluctuations. The σ_e and σ_q for the pion production reactions were then determined with the background constrained to this line. Figure 2 shows the different contributions to the measured yield from the ^{27}Al$(e,e'\pi^+)$, (γ,π^+), and (n,p) reactions at 300 MeV. The "zero point" occurs at -2.3 foils since, in addition to the target foils, the beam must also penetrate the material in front of the foils (vacuum foil, fluorescent screen and air gap).

For π^- production we found a considerable contamination from the (p,n) reaction at 131 MeV and, within the errors, the yield increased linearly with target thickness. This is not unexpected because of the short range of the protons, which are produced chiefly in the giant resonance region. In this case it was not possible to calculate the (p,n) background. The energy dependence of the background was assumed to be the same as for the comparable (γ,p) reaction. With this assumption the background yield was calculated as above.

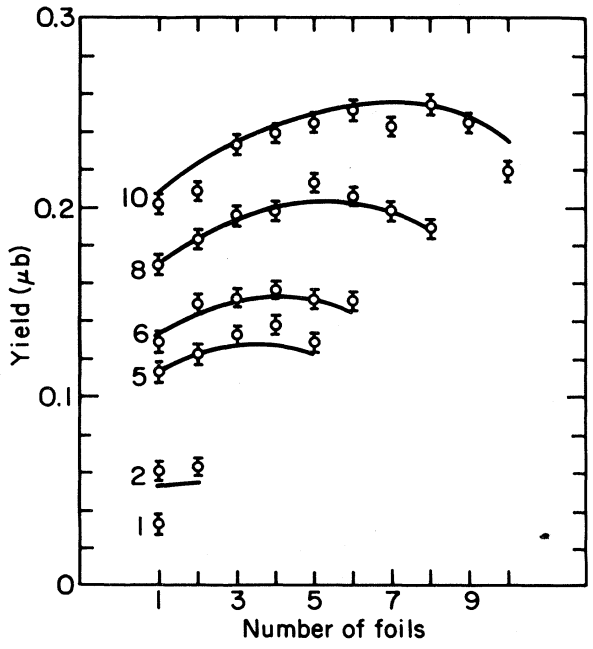

FIG. 1. Yield of ^{27}Mg versus number of foils for stacks of different thicknesses at incident electron energy $E_0 = 131$ MeV. Open circles are experimental data. The curves give the calculated yields.

III. EXPERIMENTAL RESULTS

In Figs. 3–5 we have plotted as a function of incident electron energy the measured cross sections σ_q and σ_e for the reactions ^{27}Al(γ,π^+), ^{27}Al$(e,e'\pi^+)$ and ^{51}V$(\gamma,\pi^\pm)$, ^{51}V$(e,e'\pi^\pm)$. The error bars represent random errors. In addition, there are systematic errors arising from uncertainties in decay data, sample-detector solid angle, detector efficiency, beam monitoring, and background subtraction, the last of which is the most important. Total systematic error is estimated to be about 15%.

The ratios σ_q/σ_e for ^{27}Al(γ,π^+), ^{27}Al$(e,e'\pi^+)$ and

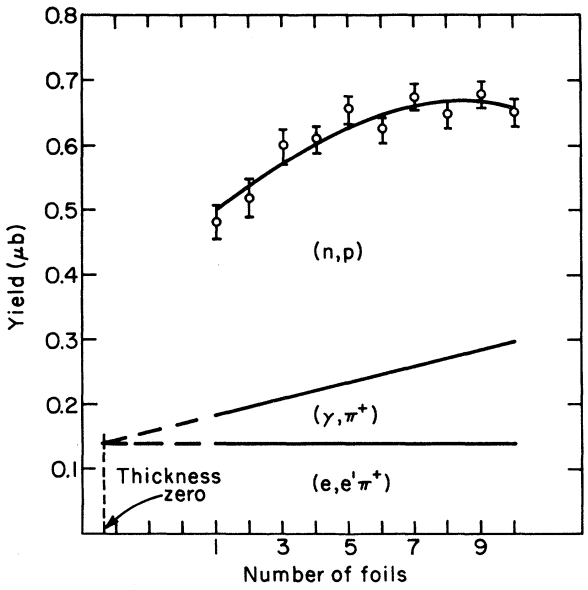

FIG. 2. Contributions to total reaction yield from the reactions Al$(e,e'\pi^+)$, (γ,π^+), and (n,p) at $E_0 = 300$ MeV. Open circles are the present experimental data.

$^{51}V(\gamma,\pi^+)$, $^{51}V(e,e'\pi^+)$ are also shown in the figures. Our value of this ratio for Al is approximately three times that of Noga *et al.*,[17] who found a ratio of 23 ± 7 in the energy region 150–270 MeV. We return to this point shortly.

The cross section per photon, σ_k, is related to σ_q by

$$\sigma_q(E_0)=\int_0^{E_0}\sigma_k(k)S(E_0,k)dk, \qquad (3.1)$$

where $S(E_0,k)dk$ is the number of bremsstrahlung quanta in the interval between k and $k+dk$ per equivalent quantum produced in the target. The cross sections σ_k were obtained from this equation by use of the Tesch smoothing method[21] and are shown as solid curves in Figs. 6 and 7 for $^{27}Al(\gamma,\pi^+)$ and $^{51}V(\gamma,\pi^+)$, respectively. Errors of $\pm20\%$ are indicated.

Our cross section for $^{27}Al(\gamma,\pi^+)$ is approximately half that found by Nydahl and Forkman[13] and Noga *et al.*,[17] but is in rough agreement with the earlier data of Walters and Hummel.[12] Above the resonance, our cross section drops rapidly with increasing energy whereas the Nydahl cross section remains constant in the energy range 300–500 MeV. For $^{51}V(\gamma,\pi^+)$ we find a resonance size and shape similar to that of Nydahl. Again, however, in the tail region, our cross section is falling to zero while the Nydahl results remain at

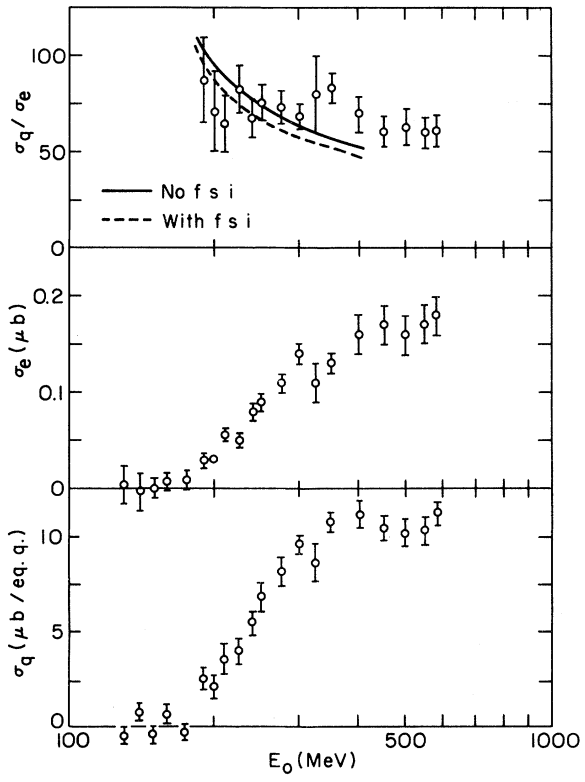

FIG. 3. Bremsstrahlung cross section per equivalent quantum σ_q and electron cross section σ_e and ratio σ_q/σ_e as a function of electron energy for the reactions $^{27}Al(\gamma,\pi^+)^{27}Mg$ and $^{27}Al(e,e'\pi^+)^{27}Mg$. See text for theoretical curves.

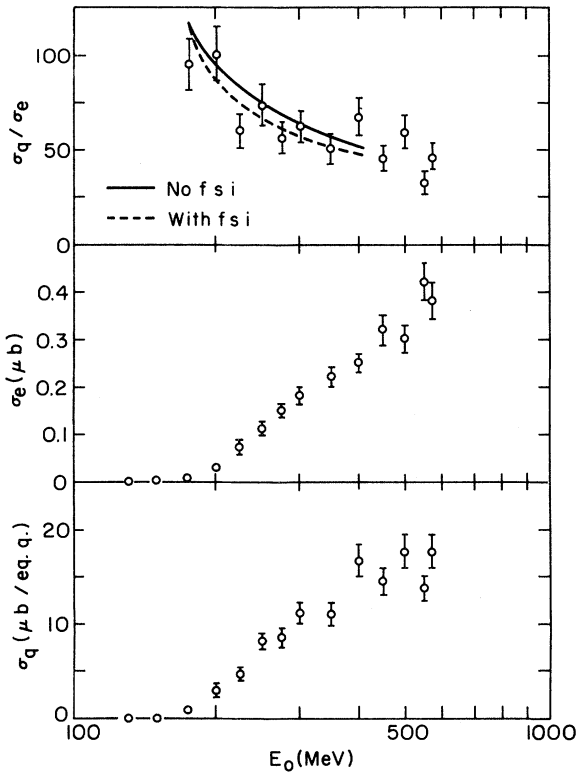

FIG. 4. Same as Fig. 3 for the reactions $^{51}V(\gamma,\pi^+)^{51}Ti$ and $^{51}V(e,e'\pi^+)^{51}Ti$.

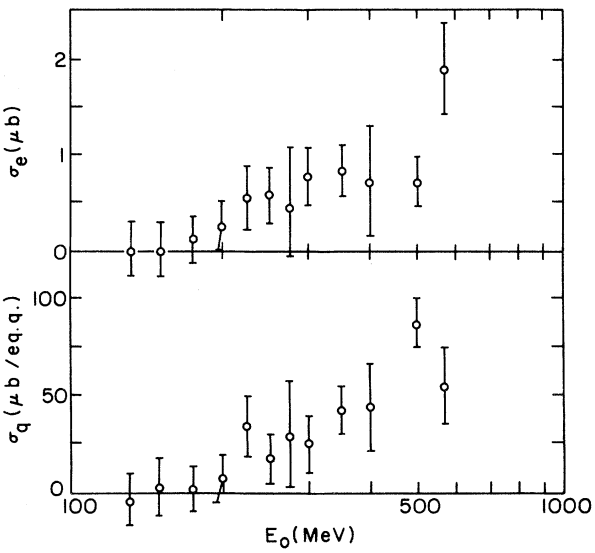

FIG. 5. σ_q and σ_e for the reactions $^{51}V(\gamma,\pi^-)^{51}Cr$ and $^{51}V(e,e'\pi^-)^{51}Cr$. See Fig. 3.

almost peak value to 500 MeV. This "post-peak constancy" is also found in the more recent results of Blomqvist *et al.*,[14] although here the peak is 40% higher and occurs 50 MeV lower than for us. The most likely explanation of the disagreement between our data and those of earlier workers is the underestimation or neglect by the latter of background reactions within the target. Even in the case of very thin targets, we showed above that these effects can be quite significant.

For the reaction $^{51}V(\gamma,\pi^-)$, no accurate cross section could be deduced because of the large errors in the yield curve arising from the long half-life and short irradiation time. In Fig. 11, we plot the cross section ratio $\sigma(\pi^-)/\sigma(\pi^+)$ which can be obtained directly from the σ_a and σ_e curves. From either photoproduction or electroproduction a mean ratio of 4 ± 2 is found for the energy region studied.

IV. THEORY

In this section we outline the calculation of the total cross section for charged pion photoproduction to bound states of the residual nucleus. We will work in the framework of the distorted wave impulse approximation and include fsi through an optical potential.

The lab cross section is given by[22] ($\hbar = c = 1$)

$$\sigma_k = (2\pi)^4 \int d\vec{p}\,\delta\left[k - (p^2+\mu^2)^{1/2} - E_f - \frac{q^2}{2M_f}\right] \times |T_{fi}(\vec{p},\vec{k})|^2, \quad (4.1)$$

in terms of the pion momentum $\vec{p}$, photon momentum $\vec{k}$, and momentum transfer $\vec{q} = \vec{k} - \vec{p}$, all in lab coordinates. The excitation energy and mass of the final nucleus are denoted E_f and M_f and μ is the pion mass.

In the impulse approximation the transition matrix may be written

$$T_{fi}(\vec{p},\vec{k}) = \sum_\alpha \int d\vec{p}'\, f^*(\vec{p},\vec{p}') \times [\Psi_f, e^{i(\vec{k}-\vec{p}')\cdot\vec{r}_\alpha} t_\alpha(\vec{p}')\Psi_i], \quad (4.2)$$

where Ψ_i (Ψ_f) are the initial (final) state nuclear wave functions and where

$$f^*(\vec{p},\vec{p}') = \frac{1}{(2\pi)^{3/2}} \int d\vec{r}\, e^{i\vec{p}'\cdot\vec{r}} \phi^{(-)}(\vec{r},\vec{p})^* \quad (4.3)$$

is the Fourier transform of the π-nucleus scatter-

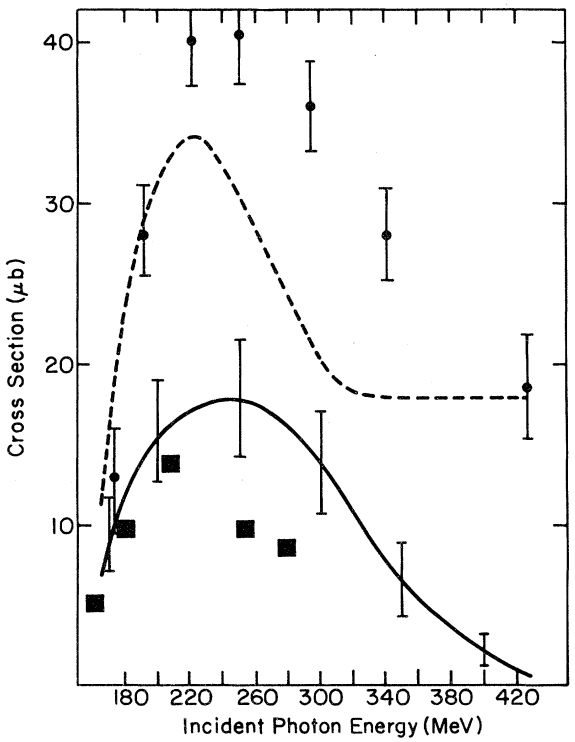

FIG. 6. Experimental cross sections per photon for the reaction $^{27}Al(\gamma,\pi^+)^{27}Mg$. The solid curve with error bars is the result of the present work. Circles with error bars are the data of Ref. 17. The dashed curve is the work of Ref. 13. The full squares are the work of Ref. 12. Reaction threshold is 142 MeV.

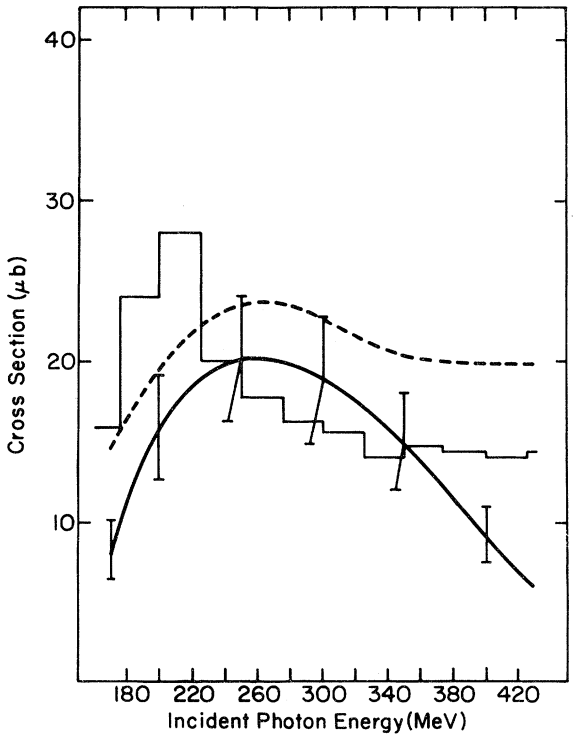

FIG. 7. Experimental cross sections per photon for the reaction $^{51}V(\gamma,\pi^+)^{51}Ti$. The solid curve with error bars is the result of the present work. The dashed curve is the work of Ref. 13. The histogram represents the data of Ref. 14.

ing state wave function. The free $\gamma\pi N$ amplitude t_α is written in the π-nucleon c.m. system[22]

$$t = i\vec{\sigma}\cdot\vec{\epsilon}F_1 + (\vec{\sigma}\cdot\vec{k})\vec{\sigma}\cdot(\vec{K}\times\vec{\epsilon})F_2 + i(\vec{\sigma}\cdot\vec{K})(\vec{k}\cdot\vec{\epsilon})F_3 + i(\vec{\sigma}\cdot\vec{k})(\vec{k}\cdot\vec{\epsilon})F_4, \quad (4.4)$$

in terms of the photon polarization $\vec{\epsilon}$, nucleon spin $\vec{\sigma}$, and unit vectors $\vec{k}$ and $\vec{K}$ in the direction of pion and photon c.m. momenta. We have chosen the gauge $\vec{\epsilon}\cdot\vec{K}=0$ and suppressed isospin. In these variables, the c.m. scattering angle is given by $\vec{k}\cdot\vec{K}=\cos\theta$.

The amplitudes F_i are decomposed into electric and magnetic multipoles, only those components being retained which are likely to contribute at photon energies less than 500 MeV. We find

$$F_1 = E_{0+} + E_{2-} + 3\cos\theta(E_{1+} + M_{1+}), \quad (4.5a)$$

$$F_2 = 2M_{1+} + M_{1-}, \quad (4.5b)$$

$$F_3 = 3E_{1+} - 3M_{1+}, \quad (4.5c)$$

$$F_4 = -3E_{2-}, \quad (4.5d)$$

where the individual multipoles including isospin are found in the tabulation of Berends, Donnachie, and Weaver (BDW).[23] Before we can use the BDW results we must Lorentz transform to the lab system and also take into account the difference in definition between our S matrix and that of BDW. We have used the definition

$$S_{fi} = \delta_{fi} - 2\pi i\delta^4(P_f - P_i)T_{fi}, \quad (4.6)$$

while BDW use

$$S_{fi} = \delta_{fi} - (2\pi)^{-2}i\delta^4(P_f - P_i)\left(\frac{m^2}{4E_\gamma E_\pi E_N E_{N'}}\right)^{1/2} T_{fi}^{\mathrm{BDW}}. \quad (4.7)$$

P_i and P_f are initial and final four-momenta, m is the nucleon mass, and the E's are the c.m. energies of photon, pion, and initial and final nucleon. We find from invariance of the total cross section that use of the BDW amplitudes requires that each multipole contribution above must be multiplied by the factor

$$\beta = \frac{W}{(2\pi)^2(E_\gamma E_\pi E_N E_{N'})^{1/2}}, \quad (4.8)$$

where the (Lorentz-invariant) total energy W is given by

$$W = [m(m + 2E_\gamma)]^{1/2}, \quad (4.9)$$

and where all energies E_i are now in the lab.

At this point we make two approximations. First, we neglect the zero-point motion of the nucleons in the nucleus. Second, we replace $t_\alpha(\vec{p}')$ in Eq. (4.2) by its on-shell value $t_\alpha(\vec{p})$. Concerning approximation 1, it would clearly be preferable to write the nuclear wave functions in momentum space and carry out the required averages explicitly. For reasons discussed in Sec. V we feel that this procedure is premature at the present time. A second alternative to the inclusion of Fermi motion is to use various fixed choice(s) of average momenta in evaluating Eq. (4.2). This method is arbitrary, however, and it is not clear to what extent it represents any real improvement over our approach. Concerning the second approximation, it has been shown[24] that t_α is a very slowly varying function of momentum even in the neighborhood of the (3, 3) resonance. Going on shell should therefore not be an unreasonable approximation.

We now expand the wave functions for the photon

$$e^{i\vec{k}\cdot\vec{r}} = 4\pi\sum_{LM_L} i^L j_L(kr)Y^*_{LM_L}(\vec{k})Y_{LM_L}(\vec{r}), \quad (4.10)$$

and distorted pion

$$\phi^{(-)}(\vec{r},\vec{p})^* = (2\pi)^{-3/2}4\pi(pr)^{-1} \times\sum_{lm} i^l e^{i(\sigma_l+\delta_l)}\phi_l(pr)Y^*_{lm}(-\vec{p})Y_{lm}(\vec{r}). \quad (4.11)$$

The pion radial wave function vanishes at $r=0$ and goes asymptotically like $\sin[pr - \frac{1}{2}(l\pi) - \eta\ln 2pr + \sigma_l + \delta_l]$. Here σ_l and δ_l are the Coulomb and strong interaction phase shifts. Inserting Eqs. (4.3), (4.10), and (4.11) into (4.2), performing the $\vec{p}'$ integration, and averaging over photon polarization and nuclear spin, we find for the total cross section (including recoil):

$$\sigma_k = \frac{4M_f(2\pi)^3}{2J_i+1}\frac{m+2k}{k^2}\int dp\frac{p}{[p^2+\mu^2]^{1/2}[m^2 - 2M_f(E_f - k + (p^2+\mu^2)^{1/2})]^{1/2}}\sum_{n\lambda Km} M^{nn}_{\lambda\lambda}(p,u_i)\frac{1}{2K+1} \times\left|\sum_{l\gamma L} i^{L-l}[(2l+1)(2\gamma+1)]^{1/2}C^{\gamma lL}_{000}C^{\gamma lL}_{-mm0}C^{\gamma nK}_{m\lambda M}e^{i(\sigma_l+\delta_l)}Y_{l-m}(u_i,0)\left\langle J_f\left\|\sum_\alpha R_l(pr_\alpha)j_L(kr_\alpha)S^\alpha_{\gamma nK}\tau^\pm_\alpha\right\|J_i\right\rangle\right|^2. \quad (4.12)$$

All indices in this expression except n and λ take on all values allowed by angular momentum coupling. The index n assumes only the values 0 and 1 and for each value of n,λ takes on the integral values $-n\le\lambda\le n$. We have used $S_{\gamma nK}$ to represent the tensor product $[Y_\gamma(\vec{r})\otimes\sigma_n]^K$ with $\sigma_0=1$ and $\sigma_1=\vec{\sigma}$. The operator $\tau^\pm$ is the usual isospin raising or lowering operator.

The term $M^{m}_{\lambda\lambda}$ contains information on the single-nucleon production amplitudes. The four contributing combinations are found to be

$$M^{00}_{00}=\tfrac{1}{2}\sin^2\theta|F_2|^2, \tag{4.13a}$$

$$M^{11}_{11}=\tfrac{1}{2}[\,|F_1|^2+\cos^2\theta|F_2|^2+\tfrac{1}{2}\sin^4\theta|F_4|^2 + \sin^2\theta\,\mathrm{Re}(F_1^*F_4)-2\cos\theta\,\mathrm{Re}(F_1F_2^*) - \sin^2\theta\cos\theta\,\mathrm{Re}(F_2^*F_4)], \tag{4.13b}$$

$$M^{11}_{00}=\tfrac{1}{2}\sin^2\theta[\,|F_2+F_3|^2+\cos^2\theta|F_4|^2 + 2\cos\theta\,\mathrm{Re}(F_2F_4^*+F_3F_4^*)], \tag{4.13c}$$

$$M^{11}_{-1-1}=M^{11}_{11}. \tag{4.13d}$$

The angle $u_i=\cos\theta_i$ is given by

$$u_i=\frac{M_f}{kp}\left[\frac{p^2+k^2}{2M_f}+E_f-k+(p^2+\mu^2)^{1/2}\right]. \tag{4.14}$$

This value arises from the δ function in Eq. (4.1). Equivalently, one could go slightly off shell, using a value of u_i derived from energy conservation in the single-nucleon process. We have done the calculation both ways and find that the two approaches lead to results differing by a few percent.

The reduced matrix element in Eq. (4.12) involves the pion distorted waves as well as all the nuclear physics. The pion wave functions $R_l(pr)=\phi_l(pr)/pr$ are assumed to arise from a potential having Coulomb and strong interaction components. The Coulomb potential is that of a uniform sphere of charge of radius 3.90 fm ($A=27$) and 4.63 fm ($A=51$). Three of the most commonly used forms were taken for the π-nucleus optical potential: (1) standard Kisslinger[25]; (2) local Laplacian[26]; (3) modified Kisslinger.[27] Woods-Saxon matter densities were used for all three potentials. For $A=27$ a half-density radius of 2.93 fm and skin thickness of 2.78 fm were assumed; for $A=51$, the corresponding numbers were 3.94 and 2.22 fm. In all cases proton and neutron distributions were assumed equal. For $T_\pi\geq 50$ MeV, the s- and p-wave scattering amplitudes were taken from Sternheim and Auerbach,[28] who Fermi-averaged the 1968 CERN phase-shift data. Higher-order partial waves were included there by renormalizing the s-wave amplitude. For $T_\pi<50$ MeV, the amplitudes were determined by extrapolating to the mesonic atom data.[2] Finally, with the potential fixed, the resulting Klein-Gordon equation was integrated numerically by use of the program PIRK.[29]

Although we will take up in the next section the explicit evaluation of the reduced matrix element for the cases of interest, we would like to make one point here concerning the sum over α in Eq. (4.12). That sum goes, in principle, over both valence and core nucleons. However, transitions out of the core will leave the residual nucleus excited above particle threshold. Although transitions to continuum states do occur and, in fact, are favored over transitions in which the final nucleus remains bound, they will not contribute to cross sections measured by activation methods which effectively sum only over particle-stable states. As a result the α summation in Eq. (4.12) is taken only over valence nucleons.

V. COMPARISONS BETWEEN THEORY AND EXPERIMENT

In this section we will compare the results of theory and experiment for the three photoproduction reactions $^{27}\mathrm{Al}(\gamma,\pi^+)^{27}\mathrm{Mg}$, $^{51}\mathrm{V}(\gamma,\pi^+)^{51}\mathrm{Ti}$, and $^{51}\mathrm{V}(\gamma,\pi^-)^{51}\mathrm{Cr}$. The relevant nuclear physics will be taken up for each case separately. Calculation of the quantity σ_q/σ_e, the ratio of the bremsstrahlung-induced to electron-induced yields, will also be described and compared with experiment.

A. $^{27}\mathrm{Al}(\gamma,\pi^+)^{27}\mathrm{Mg}$

The mass-27 isobars occupy a transition region between nuclei having prolate and oblate deformations. Over the years several models have been used to explain the experimental data with varying success. Although most of these models are collective in nature (strong coupling,[30] weak coupling,[31] rotation-vibration coupling[32]), reasonable success has also been achieved by shell model calculations carried out in large dimensional spaces.[33]

In principle, any or all of these approaches could be used to describe the states in which we are interested. What we shall do however is assume that the low-lying states of ^{27}Al and ^{27}Mg can be well represented by a small number of valence nucleons coupled to an inert ^{28}Si core. In view of the findings presented below, it will be clear that no qualitative changes in our conclusions are likely to result from this choice.

More precisely, we assume that ^{28}Si contains filled $d_{5/2}$ proton and neutron single-particle states. Transitions can then occur from the ^{27}Al ground state, represented by a $d_{5/2}$ proton hole, to the bound states of ^{27}Mg, represented as antisymmetric combinations of the configuration $|(d_{5/2p})^{-2}[J]\otimes j_n;J_f\rangle$. Only the single-neutron levels $j_n=s_{1/2}$ and $d_{3/2}$ can be populated since only they will yield states in ^{27}Mg lying below threshold. If, for the moment, we assume that all states J_f formed by all allowed couplings of J and $j_n=s_{1/2}$ and $d_{3/2}$ lie below threshold, we find that the total cross section is a sum over 14 separate contributions arising from transitions to final states of spin $\frac{1}{2}^+\leq J_f\leq\frac{11}{2}^+$.

Denoting $R_l(pr_\alpha)j_L(kr_\alpha)S^\alpha_{\gamma nK}\tau^-_\alpha$ as $O^\alpha_{lL\gamma nK}$, we find for the reduced matrix element in Eq. (4.12)

$$\left\langle J_f \left\| \sum_\alpha O^\alpha_{lL\gamma nK} \right\| J_i \right\rangle = \frac{1}{\sqrt{3}} \langle j_n \| O \| d_{5/2} \rangle, \quad J=0,$$

$$= (-)^{J_f - 1/2 + K} [2(2J_f+1)(2J+1)]^{1/2} \begin{Bmatrix} j_n & J_f & J \\ \frac{5}{2} & \frac{5}{2} & K \end{Bmatrix} \langle j_n \| O \| d_{5/2} \rangle, \quad J=2,4. \tag{5.1}$$

The single-particle matrix element is

$$\langle j_n \| O \| d_{5/2} \rangle = (-)^{l_n} \left[\frac{60(2j_n+1)(2l_n+1)(2K+1)(2\gamma+1)(2n+1)}{4\pi} \right]^{1/2} \begin{Bmatrix} l_n & \frac{1}{2} & j_n \\ 2 & \frac{1}{2} & \frac{5}{2} \\ \gamma & n & K \end{Bmatrix} \begin{pmatrix} l_n & \gamma & 2 \\ 0 & 0 & 0 \end{pmatrix}$$

$$\times \int_0^\infty R^*_{n_n l_n}(r) R_l(pr) j_L(kr) R_{12}(r) r^2 dr. \tag{5.2}$$

Oscillator wave functions of length $b = 1.84$ fm were used.

It is possible that inclusion of all allowed final states J_f may tend to overestimate the cross section. This conclusion is based on a shell model calculation we have carried out on ^{27}Mg, again assuming an inert ^{28}Si core. In this calculation, single-neutron levels were taken from the experimental spectrum of ^{29}Si and proton-hole–proton-hole and proton-hole–neutron matrix elements were derived from the spectra of ^{26}Mg and ^{28}Al, respectively. Although it is clear that such a calculation cannot yield detailed results to be compared with experiment, it may give some indication as to how much of the $(d_{5/2p})^{-2}$ strength lies in particle-stable states. We find that all of the $s_{1/2}$ neutron strength and all of the $|J=0,2\otimes d_{3/2n}\rangle$ strength lies below threshold. In contrast, almost all (~ 85%) of the $|J=4\otimes d_{3/2n}\rangle$ strength resides in unbound states. This finding will be taken into account shortly.

It will be interesting to compare our results with those for which fsi are absent. In the present formulation, the pion plane wave limit is obtained by making the replacement in Eq. (4.12) $e^{i(\sigma_l+\delta_l)} R_l(pr) \to j_l(pr)$. A far simpler approach lies in reformulating the problem in terms of the momentum transfer $\vec{q}$, in which case the infinite sum over pion partial waves can be performed analytically. This equivalence was used in earlier work by two of us[34] to investigate convergence of the sums in (4.12).

In Fig. 8 we compare our measured σ_k [curve (e)] with the theoretical results [curves (a)–(d)] for the case of plane wave pions. Curve (a) is the sum of all transitions proceeding to the $s_{1/2}$ neutron state while curve (b) represents the sum of all $d_{5/2p} \to d_{3/2n}$ transitions. The sum of (a) and (b) (not shown) is far greater than experiment over the whole range of photon energy. In curves (c) and (d) we consider the possibility that some of the $(d_{5/2p})^{-2}$ strength lies in unbound states. Curve (c) is the sum of curve (a) and that part of (b) involving only final states $|0\otimes d_{3/2}\rangle$ and $|2\otimes d_{3/2}\rangle$. In curve (d), 25% of the cross section to states $|4\otimes d_{3/2}\rangle$ has been added to (c). It is consistent with our rough shell model calculation that the predic-

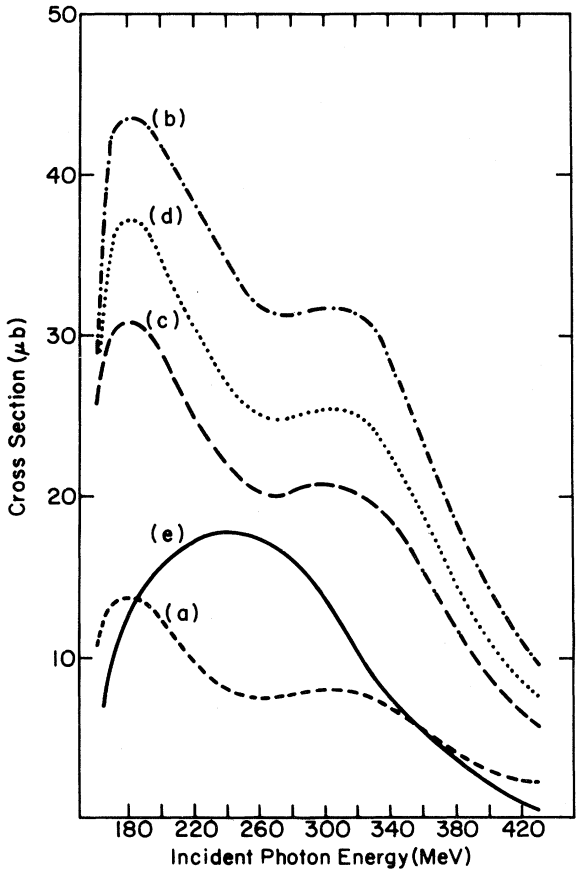

FIG. 8. Comparison of theory and experiment for the reaction ^{27}Al$(\gamma,\pi^+)^{27}$Mg. Curves (a)–(d) represent theoretical curves calculated under several assumptions (see text). Curve (e) is the result of the present measurements. All theoretical curves are calculated with fsi absent.

ted cross section for no final state interaction lies between curves (c) and (d).

We see from the figure that curves (c) and (d) are reasonably consistent with experiment (e) for $E_\gamma \geq 250$ MeV. The agreement at lower energy, however, is quite poor, both with respect to the size and shape of the cross section. We find that although the magnitude of the cross section is proportional to the number of final states populated in the reaction, the shape of the cross section to any single state is relatively state-independent. We would therefore be unable to achieve a significantly better fit to the shape of the experimental curve merely by summing over fewer final states.

In the single-nucleon process $\gamma + p \rightarrow \pi^+ + n$, $M1$ production from the (3,3) resonance dominates the spectrum to the extent that the s-wave peak appears only as a small shoulder on the low-energy side of the resonance.[35] The total cross section is similar in shape, if not in magnitude, to the experimental curve (e). In contrast, the electric dipole and magnetic dipole contributions to the present calculation are of comparable size if fsi are neglected. This relative reduction of $M1$ versus $E1$ strength arises from the nuclear kinematics and results in the characteristic two-hump pattern shown in Fig. 8 which is not observed experimentally (a similar pattern has been obtained in virtually all prior calculations which do not include fsi).

These problems pale into insignificance, however, when fsi are included (Fig. 9). Although our calculations were carried out for the three optical potentials mentioned earlier, we illustrate in curves (a)–(d) (curves have same meaning as in Fig. 8) the results using the Coulomb plus modified Kisslinger[27] potential. The other two potentials yielded very similar results.

The effect of including final state interactions is a far too strong p-wave absorption in all final states. This effect is so pronounced that curves (a)–(d) may be reproduced to with 2–3 μb by retaining in all calculations only the E_{0^+} amplitude in Eqs. (4.5). Moreover, the slight vestige of a magnetic dipole resonance which remains is shifted away from the measured peak by +50 MeV.

Faced with such a striking discrepancy, it is clear that we cannot look for a possible resolution in any of the higher-order effects (Fermi motion, binding energy corrections, etc.) which must be included in any final theory but which we have neglected here. It is also unlikely that the difficulties lie in our admittedly crude nuclear wave functions. First of all, these wave functions yielded results for plane wave pions which were reasonably consistent with experiment over a wide range of energy. Secondly, in spite of very different descriptions used for the nuclear states, fsi were found to cause the same overly strong suppression of the total cross section in three other recent calculations. The first calculation is that of Händel and Weise,[36] who used independent particle model wave functions in a calculation of $^{11}B(\gamma,\pi^-)^{11}C$. The second is that of Nagl and Überall,[37] who used Helm model wave functions in a calculation of $^{12}C(\gamma,\pi^-)^{12}N$. The third is our own work on $^{51}V(\gamma,\pi^+)^{51}Ti$ (reported in the next section), which uses realistic shell model wave functions. None of these calculations, including our own, has taken explicit account of particle-hole correlations. The existing evidence,[38] however, is that although correlations can sometimes have a strong influence on the magnitude of a cross section, they have very little effect on its shape.

We are led, therefore, to attribute the discrepancy to the optical potentials. The reactions we are studying occur on valence nucleons and for that reason take place chiefly in the vicinity of the nuclear surface. The potentials used by us and others[36,37] have all been of the Kisslinger form in

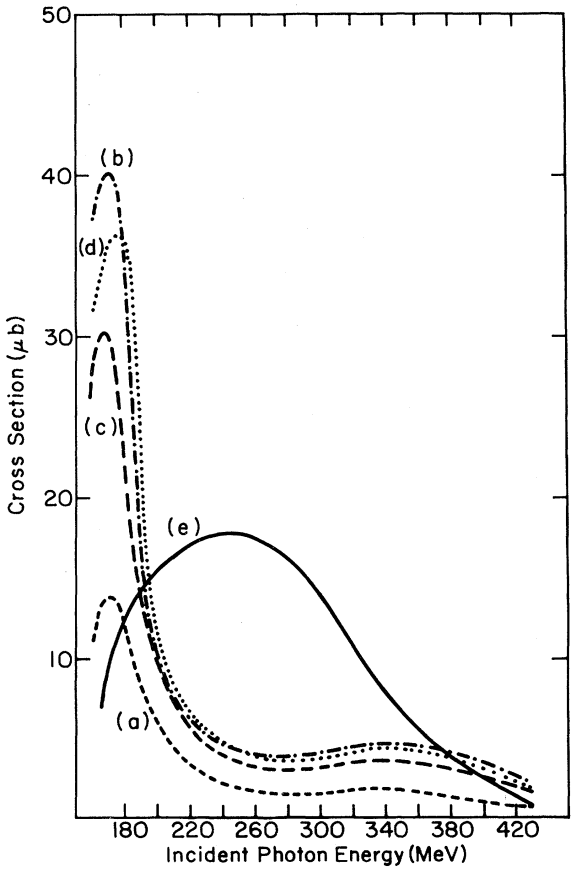

FIG. 9. Same as Fig. 8 but with fsi included. See text.

containing terms in $\vec{\nabla}\cdot\rho\vec{\nabla}$. Such potentials induce unrealistically large high momentum components in the pion wave function which could distort any type of production process,[39] especially one which peaks in the surface region. Since the gradient terms make up a large part of the absorptive component of the optical potential, their unphysical enhancement could be reflected in the too strong absorption we find here. This matter is currently under investigation.[40]

It is interesting, in view of our below-resonance results, that a recent calculation on π-nucleus elastic scattering on light nuclei[41] indicates that, at low energy, Kisslinger-type optical potentials based on the free π-N phase shifts require a much stronger s-wave repulsion if the scattering amplitude is to remain unitary. This need for an enhanced s-wave interaction has also been pointed out in pionic atom studies.[2] More generally, it is usually found that optical potentials which give good fits to the elastic scattering data in the resonance region do very poorly at lower energies.[42] Whether this can be corrected by a more accurate set of π-N phase shifts coupled with corrections to Kisslinger-type potentials[43] or whether a less restrictive potential form is necessary is not yet clear but, in either event, there are many implications here for photoproduction and electroproduction studies.

To the extent that the electron-nucleus interaction occurs via a spectrum of virtual photons,[44] the relative effects of photons and electrons in initiating photoproduction and electroproduction reactions can be evaluated given only the multipolarity of the nuclear transitions involved.[9] In the general case one can write for the electron-induced reaction cross section

$$\sigma_e(E_0)=\sum_{\mathcal{L}}\int_0^{E_0}\sigma_k(k,\mathcal{L})N_e(E_0,k,\mathcal{L})dk, \tag{5.3}$$

where $\sigma_k(k,\mathcal{L})$ represents the multipole decomposition of the photoproduction cross section and where $N_e(E_0,k,\mathcal{L})$ is the energy distribution of the virtual photon spectrum associated with the electron. Assuming a point nucleus we have[9]

$$N_e(E_0,k,\mathcal{L})=\frac{\alpha}{\pi k}\left\{\left[1+\left(\frac{E}{E_0}\right)^2\right]\ln\frac{2E_0E}{m_ek}-C_l\right\}, \tag{5.4}$$

where α is the fine structure constant, E is the energy of the scattered electron ($k=E_0-E$), m_e is the electron mass, and where

$$C_l=\begin{cases}2E/E_0, & \text{for } E1 \text{ transitions},\\ 0, & \text{for } M1 \text{ transitions},\\ -8E^2/3k^2, & \text{for } E2 \text{ transitions}.\end{cases} \tag{5.5}$$

Similarly, the bremsstrahlung-induced reaction cross section σ_q is related to σ_k by Eq. (3.1).

In the present case we have calculated σ_e by carrying out the multipole decomposition of σ_k [Eq. (4.12)] explicitly. We emphasize this point because in previous applications of this approach to pion-production processes (e.g., Ref. 17), information on the multipolarity of σ_k was unavailable, thereby necessitating the assumption that the reaction proceeded via only one multipole at all energies. By comparing the calculated σ_q/σ_e with experiment, it was hoped that information regarding the multipolarity of the interaction could be obtained. It is clear, however, in view of the dominance of $E1$ transitions at threshold and $M1$ transitions in the resonance region that such an approach is doubtful for pion-production reactions.

We illustrate in Fig. 3 the results of our calculations for σ_q/σ_e. For σ_q [Eq. (3.1)] we have taken $S(E_0,k)$ to be the standard Bethe-Heitler distribution with complete screening.[45] The σ_k used corresponds to curves (c) in Figs. 8 and 9 for the "no fsi" and "with fsi" cases, respectively. We see, in marked contrast to σ_k, that σ_q/σ_e is quite insensitive to the presence of fsi, the two results differing by a uniform 10% over the entire energy range. Again in contrast to the case of σ_k, the results are in reasonable agreement with experiment. Although comparison of bremsstrahlung- and electron-induced cross sections may in general enable one to establish consistency between photon-induced and electron-induced energy distributions, the insensitivity of σ_q/σ_e to details of the photoproduction cross section makes this quantity of limited usefulness in pion production reactions.

B. ^{51}V(γ,π^+)^{51}Ti

Because of the rigidity of ^{48}Ca, shell model calculations based on an inert ^{48}Ca core should be highly reliable. With this in mind, we write the ^{51}V ground state wave function as $|(f_{7/2p})^3;\frac{7}{2}^-\rangle$ and perform a shell model calculation on ^{51}Ti, using elements of the configuration $|(f_{7/2p})^2[J]\otimes j_n;J_f\rangle$ as a basis representation. The allowed neutron states j_n are $p_{3/2}$, $p_{1/2}$, $f_{5/2}$, and $g_{9/2}$. Neutron single-particle energies and proton-proton matrix elements are taken from the experimental spectra of ^{49}Ca and ^{50}Ti; neutron-proton matrix elements were obtained from shell model calculations in the $N=28$ region.[46] The resulting wave functions have been tested[46,47] on a wide variety of nuclear properties (energy levels, spectroscopic factors, magnetic moments, electromagnetic transition rates, β-decay rates, electron scattering form factors)

and found to be in good to excellent agreement with experiment. The results of the present section are therefore relatively free of the wave function ambiguities which occurred for $A = 27$.

If we write the wave functions for any of the final states $|J_f\rangle$ as $|J_f\rangle = \sum_{j_n J} b(j_n J J_f) \times |(f_{7/2})^2[J] \otimes j_n; J_f\rangle$, where the amplitudes result from the shell model calculation, we have that

$$\left\langle J_f \left\| \sum_\alpha O^\alpha_{lL\gamma nK} \right\| J_i \right\rangle = (-)^{J_f - 1/2 + K}[24(2J_f+1)]^{1/2} \sum_{j_n J} a(J) b(j_n J J_f) \begin{Bmatrix} j_n & J_f & J \\ \frac{7}{2} & \frac{7}{2} & K \end{Bmatrix} \langle j_n \| O \| f_{7/2} \rangle . \tag{5.6}$$

The $a(J)$ are cfp's arising from the antisymmetrization of $(f_{7/2})^3$. The single-particle matrix element is

$$\langle j_n \| O \| f_{7/2} \rangle = (-)^{l_n} \left[\frac{56(2j_n+1)(2l_n+1)(2K+1)(2\gamma+1)(2n+1)}{2\pi} \right]^{1/2} \begin{Bmatrix} l_n & \frac{1}{2} & j_n \\ 3 & \frac{1}{2} & \frac{7}{2} \\ \gamma & n & K \end{Bmatrix} \begin{pmatrix} l_n & \gamma & 3 \\ 0 & 0 & 0 \end{pmatrix}$$

$$\times \int_0^\infty R^*_{n_n l_n}(r) R_l(pr) j_L(kr) R_{13}(r) r^2 dr . \tag{5.7}$$

Oscillator wave functions of length $b = 2.03$ fm were employed.

Before illustrating the results, we would like to reemphasize[48] the possible need for detailed shell model calculations in photoproduction reactions which proceed to bound states. When all single-particle strength lies below particle threshold, it is sufficient to calculate only the amplitude for the corresponding single-particle transition. For example, our calculations show that virtually all the $p_{3/2}$ single-neutron strength resides below threshold (6.4 MeV) in ^{51}Ti. It would therefore be a good approximation and far simpler to calculate the cross section for the single-particle reaction $f_{7/2p} \rightarrow p_{3/2n}$ rather than sum the cross sections to those three-particle states in ^{51}Ti which contain varying amounts of $p_{3/2}$ strength. Approximately half of the $f_{5/2}$ and $g_{9/2}$ strength lies, however, in unbound states and must not be included in the calculation of σ_k. This is especially important in ^{51}Ti since, as we have pointed out earlier,[48] most of the contribution to the cross section comes from transitions to these two states. The full shell model calculation tells us what fraction of the single-particle strength lies in bound states and must be included in σ_k and what fraction lies in unbound states and should be ignored.

In Fig. 10, we show the theoretical cross sections without [curve (a)] and with [curve (b)] fsi and compare them with experiment [curve (c)]. Although the fsi are somewhat more effective at low energy in ^{51}Ti than in ^{27}Mg, the resemblance between the two sets of results is immediately apparent. It is, in fact, possible to transpose the discussion of the last section to the present case virtually *in toto*. It is encouraging that the similarity between corresponding theoretical curves for $A = 27$ and $A = 51$ is duplicated by the measured cross sections. Because the nuclear ingredients are so different in the two cases, our conclusion that nuclear factors are not the cause of the discrepancy is made more plausible.

The calculated cross section ratios σ_q/σ_e are shown in Fig. 4. The no fsi and with fsi curves were calculated using the values of σ_k correspon-

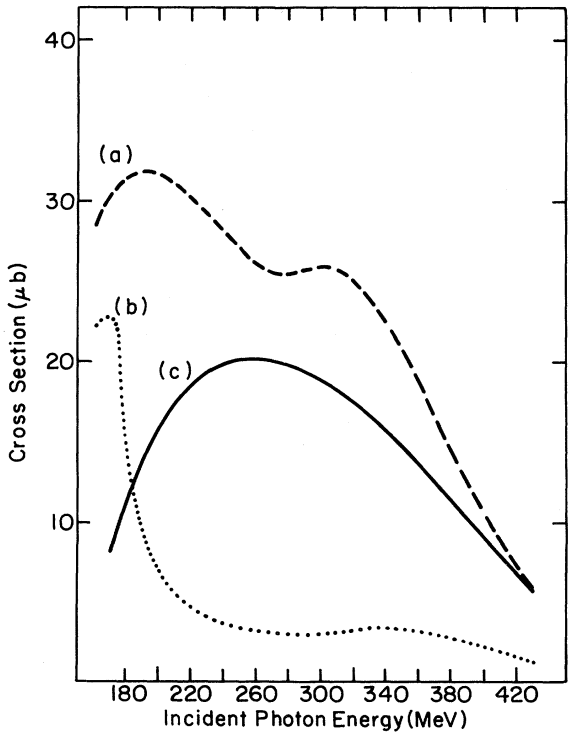

FIG. 10. Comparison of theory and experiment for the reaction ^{51}V$(\gamma, \pi^+)^{51}$Ti. Curve (a) is calculated without fsi. Curve (b) is calculated with fsi. Curve (c) is the result of the present measurements.

ding to curves (a) and (b) in Fig. 10. With respect to the effect of fsi and agreement with experiment, the results and conclusions are virtually identical to the $A = 27$ case.

C. $^{51}V(\gamma,\pi^-)^{51}Cr$

Because no accurate experimental cross section could be determined for this reaction, we content ourselves here with calculating only the non-fsi case and comparing our results with the cross section ratio $\sigma(\pi^-)/\sigma(\pi^+)$ of Fig. 11.

In this reaction, a neutron makes a transition out of a closed $f_{7/2}$ shell into any of the single-proton levels $f_{7/2}$, $p_{3/2}$, $p_{1/2}$, $f_{5/2}$, or $g_{9/2}$. Even with the three protons in ^{51}V constrained by the single-particle nature of the process to remain in the $(f_{7/2})^3$ configuration, the number of allowed couplings of four-proton to one-neutron-hole states in ^{51}Cr is extremely large. In order to keep the calculation within bounds, we observe the following. First, the neutron configurations in the lowest-lying excited states of ^{51}Cr differ from the $(f_{7/2})^8$ configuration by more than one particle and will therefore not contribute to the cross section. Second, the $\frac{7}{2}^-$ ground state will certainly contribute as will some of the higher-lying excited states, which arise from complicated couplings of extracore particles. Actual calculation shows that of the latter states the dominant contributions to σ_k originate in those configurations having a resultant spin of $\frac{7}{2}^-$.

Following these observations, we allow two types of transitions to take place. In the first, $|J_i\rangle \equiv |^{51}V \text{ ground state}\rangle \rightarrow |(f_{7/2p})^4[v,J]\otimes(f_{7/2n})^{-1};\frac{7}{2}^-\rangle$; in the second,

$$|J_i\rangle \rightarrow |\{(f_{7/2p})^3[1,\tfrac{7}{2}^-]\otimes j_p\}[J]\otimes(f_{7/2n})^{-1};\tfrac{7}{2}^-\rangle.$$

In the second transition, only the seniority-1 spin $\frac{7}{2}^-$ intermediate proton coupling can connect to the ^{51}V ground state. The allowed proton single-particle states j_p are $p_{3/2}$, $p_{1/2}$, and $f_{5/2}$; the $g_{9/2}$ is excluded from parity considerations.

In allowing only a subset of final states (those with $J_f = \frac{7}{2}^-$) to contribute to the cross section, we are ignoring the much smaller contributions from states having different spin. This is balanced, at least in part, by the assumption that a full shell model calculation would show that for all final states all the single-particle transition strength lies below threshold. To the extent that these two factors cancel each other, our restriction to two types of transitions represents a good approximation. Subsidiary calculations have been made to check this point and indicate that our results are valid to within ± 30%, well within the experimental error.

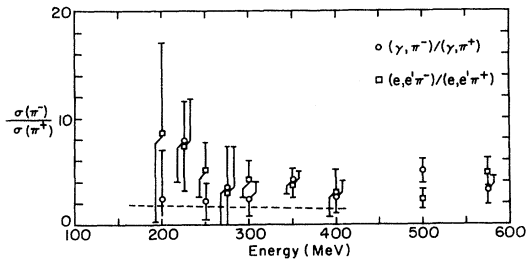

FIG. 11. Ratio of negative to positive pion electroproduction and photoproduction cross sections on ^{51}V. The dashed line is the calculated ratio with fsi absent.

After some algebra, we find for transitions of the the first type ($\tau_\alpha^- \rightarrow \tau_\alpha^+$ in the definition of $O^\alpha_{lL\gamma nK}$)

$$\left\langle J_f \left\| \sum_\alpha O^\alpha_{lL\gamma nK} \right\| J_i \right\rangle = 8[2J+1]^{1/2} \begin{Bmatrix} \frac{7}{2} & \frac{7}{2} & K \\ \frac{7}{2} & \frac{7}{2} & J \end{Bmatrix} \times (([\tfrac{7}{2})^3[1,\tfrac{7}{2}];\tfrac{7}{2}|\}(\tfrac{7}{2})^4 v J)\langle f_{7/2}\| O \| f_{7/2}\rangle. \quad (5.8)$$

For the second type

$$\left\langle J_f \left\| \sum_\alpha O^\alpha_{lL\gamma nK} \right\| J_i \right\rangle = 4(-)^{j_p+1/2}[2J+1]^{1/2} \begin{Bmatrix} \frac{7}{2} & j_p & K \\ \frac{7}{2} & \frac{7}{2} & J \end{Bmatrix} \langle j_p\| O \| f_{7/2}\rangle. \quad (5.9)$$

The single-particle matrix elements are given by expressions similar to Eq. (5.2),

Our results for the $\sigma(\pi^-)/\sigma(\pi^+)$ ratio are indicated in Fig. 11 by a dashed line. We find the ratio to be almost energy-independent, ranging from a low of 1.45 at 410 MeV to a high of 1.85 at 170 MeV. This is slightly lower than the experimental ratio of 4±2, but in view of the approximations made we consider the agreement quite reasonable.

Since the elementary cross sections $\sigma(\gamma p \rightarrow \pi^+ n)$ and $\sigma(\gamma n \rightarrow \pi^- p)$ are approximately equal in this energy region, any differences between the cross sections for $^{51}V(\gamma,\pi^+)^{51}Ti$ and $^{51}V(\gamma,\pi^-)^{51}Cr$ should be due almost entirely to structure effects. Two such effects are immediately apparent. In the former reaction, it was found that the $g_{9/2}$ single-neutron state contributed substantially to the cross section even though some of the strength lay in unbound levels. Partly because of kinematics, the $f_{7/2p} \rightarrow g_{9/2n}$ transition was actually favored[48] over $f_{7/2p} \rightarrow f_{5/2n}$ even though the corresponding β decays were first forbidden and allowed, respectively. In the π^- reaction, parity considerations forbid the $g_{9/2}$ proton state from making any contribution. On the other hand, the $f_{7/2}$ neutron shell is closed

to protons in the π^+ reaction while the $f_{7/2}$ proton shell can be populated in the π^- reaction. In particular, the strong transition $f_{7/2p} \rightarrow f_{7/2n}$ is forbidden for $^{51}V(\gamma,\pi^+)$ while the reverse transition is allowed for $^{51}V(\gamma,\pi^-)$. Although other considerations certainly enter, the rough equality of the π^+ and π^- cross sections is an indication that these two effects, going in opposite directions, are of approximately equal importance.

VI. SUMMARY AND CONCLUSIONS

Total cross section measurements for the reactions $^{27}Al(\gamma,\pi^+)^{27}Mg$, $^{27}Al(e,e',\pi^+)^{27}Mg$, $^{51}V(\gamma,\pi^+)^{51}Ti$, $^{51}V(e,e'\pi^+)^{51}Ti$, $^{51}V(\gamma,\pi^-)^{51}Cr$, and $^{51}V(e,e'\pi^-)^{51}Cr$ were carried out in the energy range 130–580 MeV. Activation methods utilizing a Ge(Li) detector were employed to measure γ activity in the target foils. Great care was taken to subtract out the considerable contributions from (n,p) and (p,n) reactions originating from neutrons and protons produced in the target. The strong disagreement between our results and those of earlier studies stems chiefly from the neglect or underestimation of these background yields in the earlier work.

Photoproduction cross sections were calculated in the impulse approximation from the region just above threshold to the (3,3) resonance tail. All pion momentum-dependent terms in the $\gamma\pi N$ amplitude and all contributing pion partial waves were retained. The individual multipoles were taken from Berends *et al.*[23] π-nucleus final state interactions were included through a variety of optical potentials whose scattering amplitudes were taken largely from Sternheim and Auerbach.[28] Theoretical cross sections were decomposed into multipoles which were used to calculate the ratio of bremsstrahlung-induced to electron-induced yields.

Comparison between theory and experiment indicates that all the optical potentials employed result in an s-wave repulsion that is too weak and a p-wave absorption which is far too strong for calculated photoproduction cross sections to be consistent with experiment. It is suggested that the gradient terms contained in the Kisslinger-type optical potentials used may artificially distort the pion wave function in such a way as to overemphasize the absorptive part of the π-nucleus interaction. The photon/electron yield ratios, although in agreement with experiment, were found to be insensitive to details of the photoproduction cross section and therefore of limited value as a critical parameter in pion-production reactions.

In contrast to coherent π^0 photoproduction, charged pion photoproduction takes place predominantly in the nuclear surface region. For this reason, it had long been felt that the effects of π-nucleus final state interactions would be minimal for charged pion processes and could be calculated quickly and subtracted out judiciously so that nuclear structure information could be obtained. Quite apart from its value in determining structural features, we have shown here that the sensitivity of pion photoproduction to final state effects makes it a potentially very effective testing ground for π-nucleus optical potentials.

This work has benefited from discussions with J. Eisenberg, K. Srinivasa Rao, G. Rawitscher, M. Sternheim, H. Überall, and C. Werntz. We are indebted to G. Miller and R. Eisenstein for assistance in using the program PIRK. One of us (N.F.) would like to thank Dr. Nils Robert Nilsson and the Nordic Accelerator Committee for supporting his visits to Lund and another (G.J.) would like to thank Professor Roland Good for assistance while he was at Penn State. We would also like to thank the Forschungskollegium at DESY for approving this experiment and for making beam facilities available. Support for the experimental work has also been provided by the Swedish Atomic Research Council.

[1] J. H. Koch and T. W. Donnelly, Nucl. Phys. B64, 478 (1973); F. Cannata *et al.*, Can. J. Phys. 52, 1405 (1974); A. Nagl, F. Cannata, and H. Überall, Phys. Rev. C 12, 1586 (1975).

[2] M. Krell and T. E. O. Ericson, Nucl. Phys. B11, 521 (1969); M. Krell and S. Barmo, *ibid.* B20, 461 (1970).

[3] F. Cannata, C. W. Lucas, Jr., and C. W. Werntz, Phys. Rev. Lett. 33, 1316 (1974).

[4] M. Ericson and M. Rho, Phys. Rep. 5, 58 (1972).

[5] M. Moreno, J. Pestieau, and J. Urias, Phys. Rev. C 12, 514 (1975).

[6] J. C. Bergstrom, I. P. Auer, and R. S. Hicks, Nucl. Phys. A251, 401 (1975).

[7] J. Deutsch *et al.* in *High-Energy Physics and Nuclear Structure—1975,* edited by D. E. Nagle *et al.* (American Institute of Physics, New York, 1975); Phys. Rev. Lett. 33, 316 (1974); C. Tzara, in Proceedings of the International Topical Conference Meson-Nuclear Physics, Carnegie-Mellon University, 1976 (unpublished).

[8] J. B. Camarata, Nucl. Phys. A254, 422 (1975).

[9] R. H. Dalitz and D. R. Yennie, Phys. Rev. 105, 1598 (1957); W. C. Barber, *ibid.* 111, 1642 (1958).

[10] P. Dyal and J. P. Hummel, Phys. Rev. 127, 2217 (1962).

[11] R. A. Meyer *et al.*, Phys. Rev. 138, B1421 (1965).

[12]W. B. Walters and J. P. Hummel, Phys. Rev. 143, 833 (1966).
[13]G. Nydahl and B. Forkman, Nucl. Phys. B7, 97 (1968).
[14]I. Blomqvist, G. Nydahl, and B. Forkman, Nucl. Phys. A162, 193 (1971).
[15]B. Friberg *et al.*, Z. Phys. 262, 255 (1973).
[16]G. Anderson *et al.*, Nucl. Phys. A197, 44 (1972).
[17]V. I. Noga *et al.*, Yad. Fiz. 14, 904 (1971) [Sov. J. Nucl. Phys. 14, 506 (1972)].
[18]W. W. Bowman and K. W. MacMurdo, At. Data Nucl. Data Tables 13, 89 (1974).
[19]I. Blomqvist *et al.*, DESY report No. 76/51 (unpublished) (obtainable through G. Jonsson).
[20]A. I. Aliev *et al.*, Handbook of Nuclear Data for Neutron Activation Analysis, Israel Program for Scientific Translations, Jerusalem, 1970 (unpublished).
[21]K. Tesch, Nucl. Instrum. Methods 95, 245 (1971).
[22]M. L. Goldberger and K. M. Watson, *Collision Theory* (Wiley, New York, 1964).
[23]F. A. Berends, A. Donnachie, and D. L. Weaver, Nucl. Phys. B4, 54, 103 (1967).
[24]L. M. Saunders, Nucl. Phys. B7, 293 (1968).
[25]L. S. Kisslinger, Phys. Rev. 98, 761 (1955).
[26]H. K. Lee and H. McManus, Nucl. Phys. A167, 257 (1971).
[27]G. A. Miller, Phys. Rev. C 10, 1242 (1974); R. Mach, Nucl. Phys. A205, 56 (1973).
[28]M. M. Sternheim and E. H. Auerbach, Phys. Rev. C 4, 1805 (1971).
[29]R. A. Eisenstein and G. A. Miller, Comp. Phys. Commun. 8, 130 (1974); also private communication.
[30]K. H. Bhatt, Nucl. Phys. 39, 375 (1962).
[31]V. K. Thankappan, Phys. Rev. 141, 957 (1966).
[32]H. Röpke *et al.*, Nucl. Phys. A156, 477 (1970).
[33]B. H. Wildenthal and J. B. McGrory, Phys. Rev. C 7, 714 (1973).
[34]N. Freed and P. Ostrander, Phys. Lett. 61B, 449 (1976).
[35]E.g., W. O. Lock and D. F. Measday, *Intermediate Energy Nuclear Physics* (Methuen, London, 1970).
[36]R. Händel and W. Weise, Lett. Nuovo Cimento 14, 592 (1975).
[37]A. Nagl and H. Überall, private communication and (unpublished).
[38]V. Devanathan and K. Srinivasa Rao, Phys. Lett. 32B, 578 (1970); A. K. Rej and T. Engeland, *ibid.* 45B, 77 (1973); K. Srinivasa Rao, (private communication).
[39]E.g., for (p,π^+) reactions, cf. G. A. Miller and S. C. Phatak, Phys. Lett. 51B, 129 (1974).
[40]N. Freed, P. Ostrander, and K. S. Rao (unpublished).
[41]M. D. Cooper and R. A. Eisenstein, Phys. Rev. C 13, 1334 (1976).
[42]M. M. Sternheim and R. R. Silbar, Ann. Rev. Nucl. Sci. 24, 249 (1974).
[43]M. Thies, in Proceedings of the International Topical Conference on Meson-Nuclear Physics, Carnegie-Mellon University, 1976 (unpublished); R. H. Landau and A. W. Thomas, Phys. Lett. 61B, 361 (1976).
[44]K. F. Weizsacker, Z. Phys. 88, 612 (1934); E. J. Williams, Phys. Rev. 45, 729 (1934).
[45]B. Rossi, *High-Energy Particles* (Prentice-Hall, New York, 1956).
[46]J. Vervier, Nucl. Phys. 78, 497 (1966); H. Horie and K. Ogawa, Prog. Theor. Phys. 46, 439 (1971).
[47]G. A. Peterson *et al.*, Phys. Rev. C 7, 1028 (1973).
[48]N. Freed and P. Ostrander, Phys. Rev. C 11, 805 (1975).